Investigation on the Long Term Behaviour of Damage Effects and Corresponding Defects in Detector Grade Silicon after Neutron Irradiation

Torsten Schulz

1995

Dissertation, Universität Hamburg, Germany

Abstract

The use of silicon detectors in high energy experiments has become common practice. However, the extremely high luminosities of the next generation experiments (e.g ATLAS and HERA-B) require systematic investigations on the radiation hardness of silicon detectors to guarantee a reasonable long term stability of their operational properties. This thesis investigates the evolution of damage effects in a long time range after neutron irradiation and characterises the induced defects.

In contrast to charged particles, neutrons cause damage mainly to the bulk of the silicon and affect the surface properties only to a minor degree. The defects generated in the bulk have considerable influence on the leakage current and the operational voltage which is governed by the effective doping concentration, respectively the space charge. The short term post-irradiation annealing of the effective doping concentration is known to be followed by a pronounced long term reverse annealing. This process has been investigated by the use of isothermal heat treatments in the temperature range between 5°C and 80°C. It is shown that the reverse annealing can be described best by a second order reaction as known from chemical processes. At temperatures below 5°C the reverse annealing is completely frozen.

Besides the defects which undergo annealing, a further type of defect has been found to contribute to the space charge the number of which is found to be constant in time after irradiation.

As opposed to the effective doping concentration the current reaches a constant level after the short term annealing. The short term annealing stages of current and effective doping concentration have been found to be rather similar. It is therefore proposed that the same type of defects are responsible for the annealing components of both current and space charge. Also the non-annealing components of current and space charge may originate from one type of defect.

In order to gain a more precise insight into the processes responsible for the damage effects it is necessary to characterise the defects caused by irradiation. Defects in semiconductors may establish energy levels in the forbidden band gap which influence the electrical properties of the material. *Deep Level Transient Spectroscopy* (DLTS) and *Thermally Stimulated Current* (TSC) were applied to classify the energy level parameters, the generation rates and annealing behaviour of the defects. Whereas the very sensitive DLTS-technique is limited to defect concentrations small in comparison with the doping concentration, the TSC-method provides good results in the cases of higher defect concentrations.

Float-zone material with different initial doping concentrations has been investigated by DLTS. Prior to irradiation up to five energy levels occur in the spectra. Four levels are found to be radiation induced. The TSC-investigations were focused on material with low doping concentrations. It is shown that the TSC-signal can be simulated properly making use of the level parameters as determined by DLTS. It is found that after high fluence exposure the evaluation of defect concentrations can be hampered by the drastic change of space charge with decreasing temperature.

Finally possible correlation of the determined defect levels and the change of detector properties are discussed.

Kurzfassung

Siliziumdetektoren finden schon seit einiger Zeit Anwendung in der Hochenergiephysik. Aber die extrem hohen Luminositäten, die in zukünftigen Experimenten (z.B ATLAS und HERA-B) zu erwarten sind, erfordern systematische Untersuchungen, inwieweit Siliziumdetektoren trotz der hohen Strahlenbelastung unter stabilen Bedingungen betrieben werden können. In dieser Arbeit werden die Langzeitauswirkungen von Schädigungseffekten nach Neutronenbestrahlung untersucht, und die erzeugten Defekte charakterisiert.

Im Gegensatz zu geladenen Teilchen verursachen Neutronen hauptsächlich Schädigung im Substrat und weniger an den Ober- bzw. Grenzflächen. Die Schädigung im Substrat hat starken Einfluß auf den Sperrstrom und die Betriebsspannung, die von der effektiven Dotierungskonzentration, bzw. der Raumladung abhängig ist.

Es ist bekannt, daß der Kurzzeitausheilung der effektiven Dotierungskonzentration eine sehr ausgeprägte, lang andauernde Anti-Ausheilung folgt. Diese Anti-Ausheilung wurde mit Hilfe von isothermalen Temperungen im Temperaturbereich zwischen 5°C und 80°C untersucht. Es wird gezeigt, daß die Anti-Ausheilung am besten beschrieben wird durch eine Reaktion zweiter Ordnung wie bei chemischen Prozessen. Unterhalb von 5°C ist die Anti-Ausheilung vollständig unterdrückt.

Neben den Defekten, die zur Raumladung beitragen und zeitlichen Veränderungen unterworfen sind, wurden auch solche gefunden, deren Konzentration sich im Laufe der Zeit nach Bestrahlung nicht ändert.

Anders als die effektive Dotierungskonzentration erreicht der Sperrstrom nach der Kurzzeitausheilung einen konstanten Wert. Für Sperrstrom und effektive Dotierungskonzentration wurden ähnliche Ausheilstufen gefunden, die den Schluß zulassen, daß jeweils derselbe Defekt verantwortlich ist für die ausheilenden Anteile beider Größen. Genauso könnten die nicht ausheilenden Anteile des Sperrstroms und der Raumladung von einem Defekttyp herrühren.

Defekte in Halbleitermaterialien erzeugen Energieniveaus in der Bandlücke, die Einfluß auf die elektrischen Eigenschaften des Materials haben. Zur Klassifizierung der Defekte nach Niveauparameter, Generationsrate und Ausheilverhalten wurden die Techniken *Deep Level Transient Spectroscopy* (DLTS) und *Thermally Stimulated Current* (TSC) angewendet. Während die Anwendung der sehr empfindlichen DLTS-Methode begrenzt ist auf Defektkonzentrationen, die klein sind im Vergleich zur effektiven Dotierungskonzentration, erreicht man mit der TSC-Methode gute Ergebnisse eher bei höheren Defektkonzentrationen.

Mit der DLTS-Methode wurde *Float-zone*-Material mit verschieden hohen Ausgangsdotierungen untersucht. Im unbestrahlten Material lassen sich bis zu fünf Energieniveaus nachweisen. Vier Niveaus werden durch die Bestrahlung generiert.

Die Untersuchungen mit der TSC-Methode wurden auf Material mit niedriger Ausgangsdotierung konzentriert. Es wird gezeigt, daß sich die TSC-Messungen unter Verwendung der DLTS-Ergebnisse sehr gut simulieren lassen. Nach Bestrahlungen mit hohen Fluenzen kann die Bestimmung der Defektkonzentration beeinträchtigt werden, weil sich die Raumladung mit fallender Temperatur drastisch ändert.

Abschließend werden mögliche Korrelationen zwischen den gefundenen Defektniveaus und den Änderungen der Detektoreigenschaften diskutiert.

List of Symbols, Abbreviations, and Technical Terms

Symbol	Property	Value / Page
A	Area of electrode	-66-
A^*	Effective Richardson constant	-42-
$\mathcal{A}$	Amplitude of an exponential function	-49-
$\mathcal{B}$	Offset of an exponential function	-49-
C	Capacitance	-12-
C_E	Equilibrium capacitance	-44-
$\mathcal{E}$	Electrical field	-10-
E_a	Activation energy	-28-
E_d	Minimum energy required for dislocation	-23-
E_C	Energy at bottom of conduction band	-6-
E_F	Fermi - level	-15-
E_g	Energy gap	-5-
E_i	Intrinsic Fermi - level	-16-
$E_{max,tr}$	Maximum energy transfer from neutron to Si-atom	-24-
E_n	Neutron energy	-24-
E_T	Trap level	-13-
E_V	Energy at top of valence band	-6-
ΔE_C	$E_C - E_T$	
ΔE_T	$E_T - E_V$ or $E_C - E_T$ resp.	-46-
ΔE_V	$E_T - E_V$	
I_f	Filling current	-145-
I_{for}	Forward current	-42-
I_{rev}	Reverse current	-11-
I_{BGC}	Bulk generation current	-11-
I_{TSC}	Thermally stimulated current	-55-
J_s	Saturation current density	-42-
ΔJ	Difference of current per volume after and prior to irradiation	-100-
$L_R - L_P$	Depth of trap filling	-53-
N_A	Concentration of acceptors	-5-
N_C	Defect concentration which is constant in time except chap. 2 where	-80-
	N_C means density of states in the conduction band	-14-
N_D	Concentration of donors	-5-
N_{eff}	Effective impurity concentration	-10-
N_{SC}	Concentration of occupied generation centres	-112-
N_T	Trap concentration	-13-
N_V	Density of states in the valence band	-14-
Q	Charge	
V	External voltage	-10-
V_{bi}	Built-in voltage	-10-
V_{fd}	Voltage of full depletion, depletion voltage	-11-
V_f	Filling voltage	-43-
W	Width of the SCR	-10-

Symbol	Property	Value / Page
a_n	nth Fourier cosine coefficient	-48-
b_A	Generation rate of acceptor-like states : N_A/Φ	-75-
b_C	Generation rate of constant defects : N_C/Φ	-81-
b_{cold}	Generation rate of annealing defects at lower T	-97-
b_n	nth Fourier sine coefficient	-48-
b_Y	Generation rate of reverse annealing defects : $N_{Y,\infty}/\Phi$	-81-
b_I	Generation rate of annealing defects, component I	-112-
b_{II}	Generation rate of annealing defects, component II	-112-
d	Thickness of the sample	-66-
$e_{n,p}$	Emission probability or rate respectively of electrons and holes	-14-
g_X	Generation rate of specific impurity X : n_X/Φ	
h	Planck constant	$6.626{\cdot}10^{-34}$ Js
$\hat{k}$	Reaction constant (explicit first order reaction)	-28-
$\tilde{k}$	Reaction constant (explicit second order reaction)	-28-
$\hat{k}_0$	Frequency factor	-27-
k_B	Boltzmann constant	$1.381 \cdot 10^{-23}$ J/K
m_0	Electron rest mass	$9.110 \cdot 10^{-31}$ kg
n	Electron concentration in the conduction band	-5-
n_i	Intrinsic carrier concentration	-5-
n_T	Concentration of occupied traps	-13-
p	Hole concentration in the valence band	-5-
p_T	Concentration of non-occupied traps except sec. 2.7 where p_T means transverse momentum	-13-
q	Electron charge	$1.602 \cdot 10^{-19}$ C
$t_{1/2}$	Half-life period	-29-
t_d	Time of delay, resp. de-excitation	-58-
t_f	Filling time	-117-
t_w	Time window	-47-
$v_{th,n,p}$	Thermal velocity of electrons or holes resp.	-14-
α	Current damage constant	-100-
Φ	1MeV neutron equivalent fluence	-24-
Φ_{eq}	1MeV neutron equivalent fluence	-24-
Φ_{inv}	Fluence at which type conversion occurs	-100-
ϵ_S	Electrical permitivity in silicon $\epsilon \times \epsilon_o$	$11.9 \cdot 8.854{\cdot}10^{-14}$ F/cm
η	Ideality factor	-42-
κ	Hardness factor	-24-
λ	Transition region $W - L_R$	-52-
$\mu_{n,p}$	Mobility of electrons and holes, resp.	-5-
ρ	Resistivity	-5-
τ_T	Trapping time constant	-36-

Abbreviation	Explanation	Page
AC	Alternating current	
ADC	Analog-digital converter	
ATLAS	A Toroidal Lhc ApparatuS	
CV	Capacitance voltage	-37-
BNL	Brookhaven National Laboratory	
DLTS	Deep level transient spectroscopy	-43-
ENB	Electrical neutral bulk	-15-
EPR	Electron paramagnetic resonance	
IV	Current voltage	-41-
NIEL	Non-ionising energy loss	-24-
PKA	Primary knock-on atom	-23-
PTB	Physikalisch-Technische Bundesanstalt	-66-
RT	Room temperature	about 21°C
SB	Surface barrier	-9-
SCR	Space charge region	-9-
SCT	Semiconductor Tracker	-20-
TSC	Thermally stimulated current	-55-
UKE	Universitätskrankenhaus Eppendorf	-66-

Technical Terms	Page
A-centre	-30-
Analysis of maxima	-48-
bistable	-32-
Constant time window	-50-
Deconvolution	-59-
Donor removal	-75-
Direct analysis	-50-
E-centre	-30-
Effective area	-39-
Flux	-67-
Passivation	-19-
Recalculation	-121-
metastable, multistable	-32-
Type inversion	-75-
Variable time window	-50-

Contents

1 Introduction **1**

2 Theory and Operation of Silicon Detectors **5**
2.1 Basic Properties of Detector Grade Silicon 5
2.2 Silicon Diodes 7
2.2.1 Rectifying Contacts 7
2.2.2 Current 11
2.2.3 Capacitance 12
2.3 Properties of Deep Energy Levels 13
2.4 The Fermi - level 15
2.5 Detector Operation 17
2.6 Manufacture of Detectors 18
2.7 Radiation Environment of the SCT 20

3 Radiation Induced Bulk Defects **23**
3.1 Defect Generation 23
3.2 Annealing of Defects 27
3.3 Review of Identified Defects 29
3.4 Electrical Properties of Bulk Defects 34

4 Experimental Methods **37**
4.1 Diode Characteristics 37
4.1.1 Capacitance Voltage Characteristics 37
4.1.2 Current Voltage Characteristics 41
4.2 Deep Level Transient Spectroscopy (DLTS) 43
4.2.1 The Principle of the DLTS-Technique 43
4.2.2 Application of the Fourier transformation 48
4.2.3 Accuracy and Limits 51
4.3 Thermally Stimulated Current (TSC) 55
4.3.1 Basic Equations and Determination of Trap Concentration . . 55
4.3.2 Determination of Energy Level Parameters 58
4.4 Heat Treatments 63
4.4.1 Isothermal Heat Treatments 63
4.4.2 Isochronal Heat Treatments 64

5 Experimental Equipment **65**
5.1 Samples, Detectors, and Devices under Test . . . 65
5.2 Irradiation Facilities . . . 66
5.3 Measurement Set-Up . . . 68
5.4 Cooling and Tempering . . . 71

6 Change of Detector Properties **75**
6.1 Results on Effective Doping Concentration . . . 75
6.1.1 Introduction . . . 75
6.1.2 The Reverse Annealing . . . 78
6.1.3 Short Term Annealing . . . 94
6.1.4 Effective Doping Concentration at Lower Temperature . . . 97
6.2 Results on Current . . . 100
6.2.1 Introduction . . . 100
6.2.2 Fluence Dependence at Room Temperature . . . 101
6.2.3 Time Dependence at Room Temperature and during the Heat Treatments . . . 103
6.2.4 Annealing at Lower Temperature . . . 106
6.3 Comparison of Current and N_{eff} Related Results . . . 110

7 Defect Characterisation **115**
7.1 Deep Level Transient Spectroscopy . . . 115
7.1.1 Introduction . . . 115
7.1.2 Energy Levels before Irradiation . . . 118
7.1.3 Energy Levels after Irradiation . . . 122
7.1.4 Fluence Dependence . . . 128
7.1.5 Time Dependence and Heat Treatment . . . 134
7.1.6 Hole Traps . . . 137
7.2 Thermally Stimulated Current . . . 139
7.2.1 Introduction . . . 139
7.2.2 Comparison between Different Methods of Analysis . . . 141
7.2.3 Dependence on Measurement Conditions . . . 143
7.2.4 Fluence Dependence . . . 151
7.2.5 Isothermal Tempering . . . 156
7.3 Correlation of Detector Properties and Defects . . . 160

8 Summary and Conclusions **165**

9 Appendix **173**

Chapter 1

Introduction

The first semiconductor detectors were made out of germanium in the beginning of the 50s. The attractive features of semiconductor detectors are linearity, good energy resolution, compactness and fast response. The earliest silicon detectors which based on surface barrier counters emerged in the 50s. As opposed to germanium detectors which have to be operated at very low temperature, silicon detectors can be used at room temperature in normal ambient. Silicon detectors came up in high energy physics due to the discovery of the J/Ψ-meson, a bound quark-antiquark state with a new quantum number called charm. Since charm events are produced rarely, strategies had to be developed which allow the suppression of non-charm events. Only silicon detectors provided the excellent spatial resolution necessary to distinguish between non-charm events containing only tracks which originated from the interaction point and the tracks originating from the charm decays which occur at a certain distance from the interaction point due to the life time of the charmed particle.

In the 80s ambitious experiments were designed which foresaw large calorimeters consisting of sandwich detectors, i.e. alternating layers of silicon detectors and metals, such as copper or lead. The only experiment which has been realised and which is still operating, is the *PLUG* calorimeter (Si/Cu) in the very forward direction of the *H1* experiment at the *HERA* collider.

In the end of the 90s a large hadron collider (*LHC*) will be realised at *CERN* in order to explore and test the standard model. The *LHC* machine will allow proton beam energies up to 8 TeV and a luminosity of about 10^{34} cm^{-2}s^{-1}. A typical detector at *LHC* essentially consists of a tracking component, a calorimeter and a muon detection system. The data acquisition and analysing systems have to be embedded compactly. The tracking detector is installed in the centre of the experiment in order to record the tracks of charged particles which are curved due to the applied magnetic field provided by superconducting coils. The radii of the curved tracks allow the determination of the particle's momentum and charge. A vertex detector is placed very close to the interaction point in order to locate the decay of short lived particles, which occur nearby the interaction point. The distance between the place of decay and the interaction point where the particle was generated is a measure of the life-time.

Silicon detectors are best suited to meet the challenges of high accuracy and efficient track measurements because of the high level of possible segmentation into

strips or pixels. Their compactness and the possibility to integrate the front-end electronics on the same chip are also advantageous.

The first vertex detectors based on silicon micro strip detectors were used successfully in the *MARK II* experiment at the Stanford Linear Collider. The first *CERN* experiments employing silicon vertex technology were *ALEPH* and *DELPHI* at the *LEP* collider. However, the operation of experiments in connection with the *LHC* machine has to meet even higher requirements which are caused by the high luminosity and the high particle momentum. Besides high precision and resolution, and a very short read-out time of about 20 ns, the most important challenge is the radiation hardness of levels up to Mega-Gray and 10^{14} neutron cm^{-2} respectively achieved per year. In the last few years, intense investigation has been focused on the radiation damage of silicon detectors in order to explore the degradation of the detector performance. Although other materials such as gallium arsenide or diamond are said to be radiation harder, silicon is still an attractive choice, because the fabrication process is developed to a high standard and reliability, which make silicon detectors commercially available at low costs.

The radiation causes damage to the bulk of the silicon as well as to the surfaces. This work investigates the long term behaviour of the bulk damage, because it has considerable influence on the leakage current and the effective doping concentration. The current causes noise, heat and also power consumption, and the effective doping concentration affects considerably the operational voltage. Neutrons are the appropriate kind of radiation to separate bulk and surface damage, because they do not affect the surfaces but only the bulk.

Due to the interaction of radiation and silicon atoms the periodic structure of the lattice is destroyed locally, i.e. silicon atoms are dislocated. A dislocated atom is called *interstitial atom*, whereas the lattice site which is empty now is called *vacancy*. The interstitials and vacancies form defect complexes which establish energy levels in the forbidden gap. Most of the defect complexes contain impurity atoms e.g. carbon or oxygen. It is not fully understood yet which types of defects cause the deterioration of the detector performance, e.g. the increase of current and the change of the effective doping concentration.

Since detector operation is foreseen to last several years the long term behaviour of these quantities is of major concern. It is known that most of the radiation induced defects anneal out with characteristic time constants. A certain amount of defects is stable or can be annealed out only at very much higher temperature respectively. The current shows a corresponding behaviour. After several annealing stages the current reaches a constant value. An opposite development has been found for the effective doping concentration, instead of annealing a so-called reverse annealing occurs. Both, the reverse annealing and the constant level of current are subject of this work, but also the preceding annealing stages are parametrised. However, the studies are most attentive to the time and temperature dependence of the reverse annealing.

The parametrisation of detector properties and their development after irradiation allows the forecasting under various operational scenarios, but it provides no tool to understand or even improve the situation. In order to gain a detailed insight into interaction between defects and detector properties it is an urgent request to characterise the defects induced by irradiation. Thus, besides the parametrisation of

the long term development of the detector properties the energy level parameters of the defects were studied systematically. Mainly the technique of *DLTS* (deep level transient spectroscopy) has been employed, because it is a very sensitve method. However, *DLTS* is limited to low fluences and hence the technique of *TSC* (thermally stimulated current) which can be used without restriction has also been applied. As far as possible the detected energy levels were correlated with the detector properties. It will be shown that the current and a fraction of the effective doping concentration are probably caused by the same defect.

For more detailed information on semiconductor particle tracking detectors the comprehensive review article of Hall [1], which has been used as a source for the above written historical excourse, shall be recommended. Radiation damage effects were recently reviewed by Borchi and Bruzzi [2]. Fundamentals of junction measurements in the study of deep energy levels in semiconductors were summarised by Grimmeiss and Ovren [3], and the corresponding experimental aspects are discussed for example by Bourgoin and Lannoo [4].

Whereas this chapter provides a general introduction, in the next chapter the basic principles of silicon are considered with respect to detector operation and technology. As an example the radiation environment of the *ATLAS* tracking detector is discussed. In chapter 3 the mechanisms of defect generation and annealing are explained as well as the way energy levels in the forbidden gap affect the detector properties. The most relevant types of defect will be reviewed. The experimental methods and the equipment are described in the chapters 4 and 5. The results concerning the radiation induced change of detector properties are presented in chapter 6, and chapter 7 contains the results of the defect characterisation obtained from *DLTS* and *TSC* studies. Finally, the results are summarised and conclusions are drawn and discussed.

Chapter 2

Theory and Operation of Silicon Detectors

2.1 Basic Properties of Detector Grade Silicon

The physical properties of silicon are known very well (see e.g. [5, 6, 7]). In the following the theoretical topics and experimental data relevant for this work are summarised.

The energy band gap of silicon is $E_g = 1.12$ eV. Already at room temperature electrons are excited from the valence band to the conduction band. The positive charges left in the valence band are called holes and contribute to the conductivity in a similar way as the electrons in the conduction band. In intrinsic [1] silicon the concentration of electrons in the conduction band n and that of holes in the valence band p is equal :

$$n = p = n_i. \tag{2.1}$$

The number of electrons and holes in silicon can be changed significantly by doping it with donors or acceptors. Donors are called those atoms which have additionally to the four electrons needed for the covalent bond one electron they "donate" to the conduction band. Hence the number of electrons in the conduction band can be as high as the number of donors. Acceptors are atoms having one electron less to form bondings to all neighbours. To complete the missing bond they "accept" an electron from the valence band, where a hole is left. Thus, also the number of holes can be as high as the number of acceptors. However, due to the *mass action law* the product of electron and hole concentration in thermal equilibrium always equals the square of the *intrinsic carrier concentration* [2] :

$$np = n_i^2. \tag{2.2}$$

The number of electrons and holes determines the *resistivity* ρ of the material. It is :

$$\rho = \frac{1}{q(n\mu_n + p\mu_p)}, \tag{2.3}$$

[1] totally pure

[2] The value of the intrinsic carrier concentration n_i in silicon at room temperature is about $10^{10} cm^{-3}$ [6].

where μ_n and μ_p are the mobilities of electrons and holes, respectively. If the concentration of donors N_D exceeds the concentration of acceptors N_A ($N_D > N_A$), the material is called *n-type* and the electrons are *majority carriers* and the holes *minority carriers*. Otherwise ($N_A > N_D$) the material is called *p-type* and holes are the majority carriers and electrons the minority carriers.

Very often phosphorus is used as a donor, and boron as an acceptor. The energy level of the phosphorus atom in silicon is very close to the conduction band, and thus even at very low temperature all phosphorus atoms are ionised ($N_D \approx n$). On the other hand, the energy level of the boron atom is very close to the valence band. Hence, all boron levels are occupied by an electron leaving the corresponding concentration of holes in the valence band ($N_A \approx p$). The *Fermi-level* E_F in terms of the effective density of states in the conduction band (N_C) and the valence band (N_V) and of the donor or acceptor concentration respectively, can be obtained from

$$E_C - E_F = k_B T \ln\left(\frac{N_C}{N_D}\right) \tag{2.4}$$

or

$$E_F - E_V = k_B T \ln\left(\frac{N_V}{N_A}\right), \tag{2.5}$$

where E_C denotes the energy at the bottom of the conduction band and E_V the top of the valence band, respectively [6]. k_B is the Boltzmann constant and T the temperature. In the intrinsic case the Fermi-level coincides with the centre of band gap, E_i. The energy levels are shown in fig. 2.1.

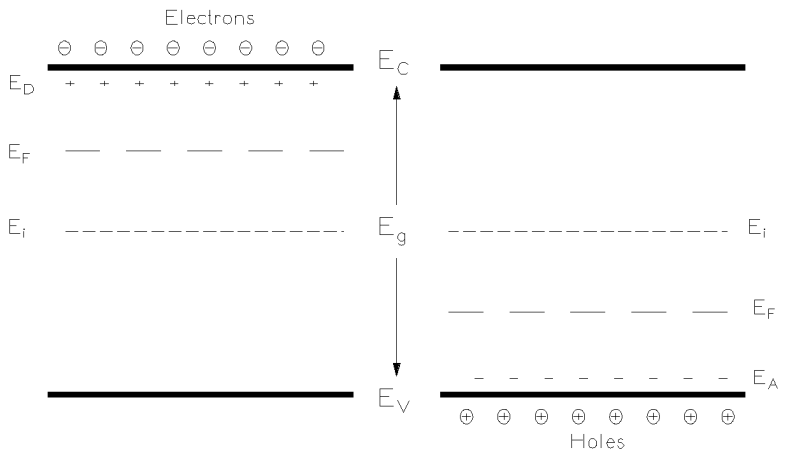

Figure 2.1: Energy diagram for n-type (left) and p-type (right) silicon. E_D denotes the energy level of the donor and E_A that of the acceptor.

Detector grade silicon has to be doped very low, i.e. its resistivity has to be very high ($N_{eff} \leq 1{\cdot}10^{12}\ cm^{-3} \hat{=} \rho > 2$ kΩcm , see sec. 2.5). In float-zone silicon which is commonly used for detector fabrication [3] [8, 9], the inevitable boron concentration

[3] The resistivity of Czochralsky grown material is too low.

is in the range of 10^{12} cm^{-3}. For the production of n-type detectors basic material with the lowest boron concentration available is chosen and then the phosphorus concentration is decreased to the required value by repeated zoning (zone refining).

Besides phosphorus and boron, a lot of other elements are found in silicon. Typical concentrations of these impurities and the corresponding detection limits are shown in fig. 2.2. While most of the impurities are present in concentrations comparable to the doping concentrations, the content of nitrogen and oxygen is much higher. The concentration of carbon in crystaline silicon ranges from 10^{15} to 10^{18} cm^{-3} [9, 10, 11].

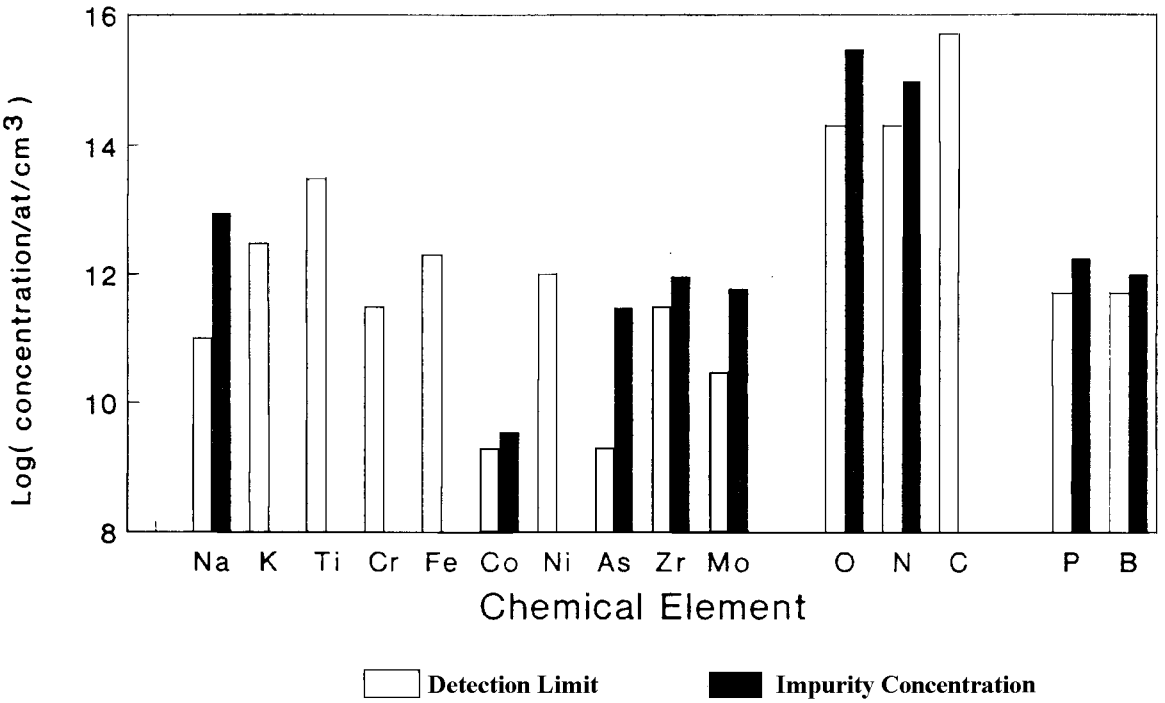

Figure 2.2: Typical impurity concentrations in float-zone silicon, determined by neutron activation analysis (left group) IR spectroscopy (O, N, C) and photoluminescence (P, B) [9].

2.2 Silicon Diodes

2.2.1 Rectifying Contacts

When the doping concentration changes abruptly from a surplus of acceptors N_A on the p-side to a surplus of donors N_D on the n-side one obtains an abrupt junction, which is called p^+-n junction if $N_A \gg N_D$. In thermal equilibrium neither electron current J_n nor hole current J_p is flowing :

$$J_n = J_p = 0. \tag{2.6}$$

From eq. 2.6 and

$$J_n = \mu_n n \frac{\partial E_F}{\partial x}, \tag{2.7}$$

respectively

$$J_p = \mu_p p \frac{\partial E_F}{\partial x}, \tag{2.8}$$

(see e.g. [6] for a detailed derivation) it follows that the Fermi-level has to be constant through the junction. Hence, the conduction band and the valence band are bent. The difference between the bottom of the conduction band on the p^+-side and its bottom on the n-side (see fig. 2.3) is called the *built-in potential*, which can also be written as

$$qV_{bi} = E_g - (qV_n + qV_b), \tag{2.9}$$

where q is the electron charge and V_n and V_b are electrical potential as explained in fig. 2.3. Corresponding to the p^+-n junction a built-in potential can be defined also for a metal semiconductor (MS) contact. For a similar reason as given for the p^+-n

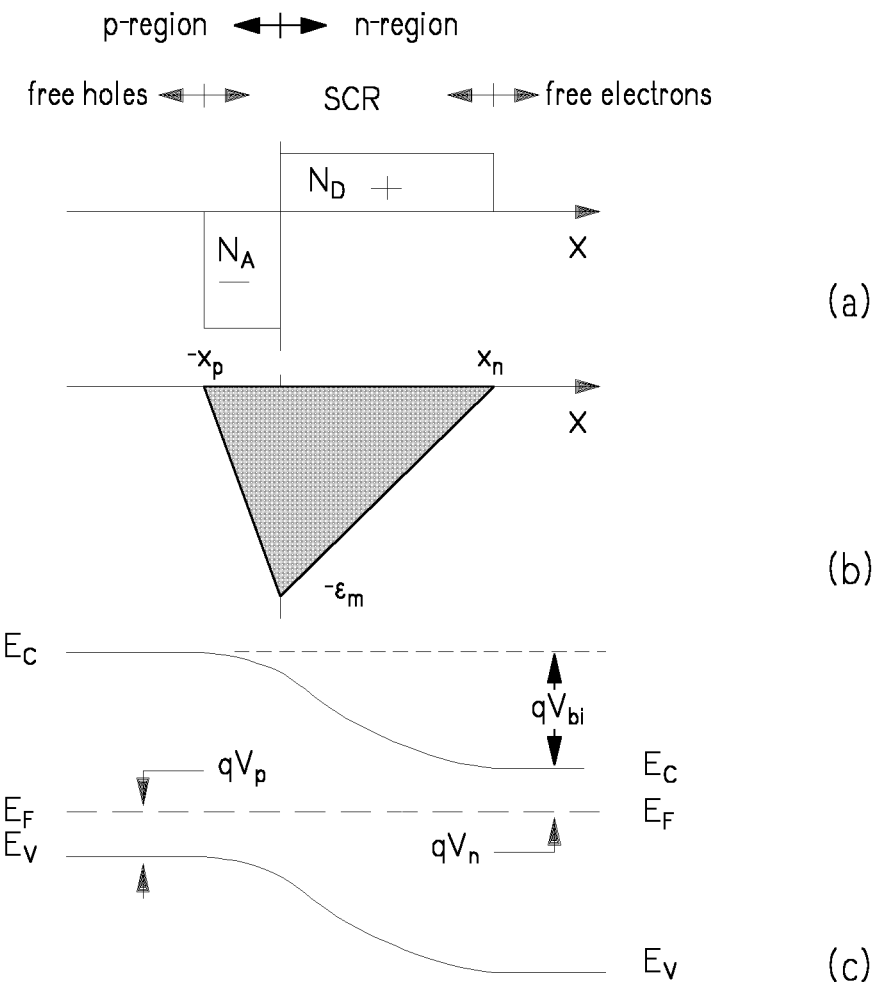

Figure 2.3: Abrupt p-n junction. (a) Space charge distribution. (b) Electric field distribution. (c) Energy-band diagram.

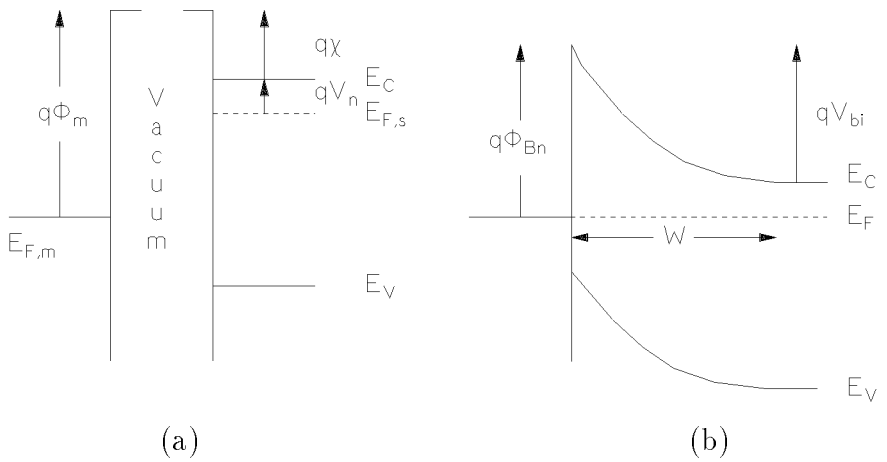

Figure 2.4: Potential barrier at the Schottky contact. Before (a) and after (b) the metal and the semiconductor are brought into intimate contact.

contact the Fermi-level of the metal and semiconductor have to coincide when both materials are brought into intimate contact. As can be seen from fig. 2.4 in the case of an n-type semiconductor a barrier height $q\Phi_{Bn}$ is established at the interface. It is limited by the difference of the metals work function Φ_m and the electron affinity $\mathcal{X}$ measured from the bottom of the conduction band to the vacuum level [4].

$$q\Phi_{Bn} = q(\Phi_m - \mathcal{X}). \tag{2.10}$$

For the MS-contact the built-in voltage can then be written as :

$$qV_{bi} = q(\Phi_{Bn} - V_n). \tag{2.11}$$

The region where the energy bands are bent is depleted of free charge carriers and thus the donors and acceptors are left uncompensated and build a space charge. Therefore this region is called *depletion region* or *space charge region* (SCR). The width of the SCR adjusts depending on the built-in voltage and the concentration of donors and acceptors. From Poisson's equation we obtain in the case of the abrupt junction and a homogenous distribution of fixed charges :

$$-\frac{\partial^2 V}{\partial x^2} \equiv \frac{\partial \mathcal{E}}{\partial x} = \frac{\rho(x)}{\epsilon_S} = \frac{q}{\epsilon_S}\left(N_D(x) - N_A(x)\right). \tag{2.12}$$

For $0 < x \leq x_n$ it is :

$$-\frac{\partial^2 V}{\partial x^2} = \frac{q}{\epsilon_S} N_D, \tag{2.13}$$

and for $-x_p \leq x < 0$:

$$-\frac{\partial^2 V}{\partial x^2} = -\frac{q}{\epsilon_S} N_A, \tag{2.14}$$

[4] The barrier height might be affected also by interface states (see e.g. [12, 13]).

(see fig. 2.3 for explanation of x_n and x_p). First integration of eqs. 2.13 and 2.14 leads to the electrical field, which is for $-x_p \leq x < 0$:

$$\mathcal{E} = \frac{-qN_A(x + x_p)}{\epsilon_S}, \tag{2.15}$$

and for $0 < x \leq x_n$:

$$\mathcal{E} = \frac{qN_D(x - x_n)}{\epsilon_S}. \tag{2.16}$$

Integrating eq. 2.12 twice one gets the built-in potential :

$$V_{bi} \equiv \frac{1}{2}\mathcal{E}_m W, \tag{2.17}$$

where $W = x_n + x_p$ is the total width of the depletion region and $\mathcal{E}_m$ is the maximum field that exists at $x = 0$:

$$|\mathcal{E}_m| = \frac{qN_A x_p}{\epsilon_S} = \frac{qN_D x_n}{\epsilon_S}. \tag{2.18}$$

Because $x_p \ll x_n \approx W$ eq. 2.17 and eq. 2.18 can be combined to

$$V_{bi} = \frac{qN_D W^2}{2\epsilon_S}. \tag{2.19}$$

The same result for the built-in voltage can be obtained if the same procedure is applied to the MS contact. Thus in both cases, p^+-n junction and MS contact, the width of the SCR can be written as

$$W = \sqrt{\frac{2\epsilon_S}{qN_D} V_{bi}}. \tag{2.20}$$

Because in high resistivity material the donor and acceptor concentration are of the same order of magnitude, N_D has to be replaced by the difference of the donor and acceptor concentration on the n-side :

$$N_{eff} = |N_D - N_A|, \tag{2.21}$$

which is the *effective doping concentration* or the effective space charge concentration.

The Debye-tail of the carrier distribution at the edges of the depleted zone is described by a term $k_B T/q$ and thus the exact expression for the width of the SCR is

$$W = \sqrt{\frac{2\epsilon_S}{qN_{eff}} \left(V_{bi} + \frac{k_B T}{q} \right)}. \tag{2.22}$$

The width of the SCR can be changed if an external voltage V is applied to the diode. It is :

$$W(V) = \sqrt{\frac{2\epsilon_S}{qN_{eff}} \left(V_{bi} + \frac{k_B T}{q} + V \right)}. \tag{2.23}$$

For voltages great in comparison with $V_{bi} + (kT/q)$ [5] a simplified expression neglecting this term can be used for the dependence of the SCR-width on the applied voltage :

$$W(V) = \sqrt{\frac{2\epsilon_S}{qN_{eff}}V}. \tag{2.24}$$

The minimum voltage needed for full depletion V_{fd} is called *depletion voltage* and can be deduced from eq. 2.24 replacing $W(V)$ by the detector thickness d :

$$V_{fd} = \frac{qN_{eff}d^2}{2\epsilon_S} \tag{2.25}$$

Knowing both d and V_{fd} it becomes possible to calculate the effective space charge concentration N_{eff}:

$$N_{eff} = \frac{2\epsilon_S}{q}\frac{V_{fd}}{d^2}. \tag{2.26}$$

2.2.2 Current

When a diode is reverse biased only a small current is flows, called *leakage current* or *reverse current* I_{rev}. It can be divided into two parts : bulk generation current I_{BGC} and surface current I_{SC}. In thermal equilibrium electron-hole pairs are generated and annihilated continuously and no net current flows. However, due to an applied reverse bias the recombination is suppressed and therefore a reverse current occurs. The generation can be greatly increased by energy levels in the centre of the band gap and is strongly temperature dependent (see sec. 4.1.2). Those centres, mainly impurities and dislocations, are found in the bulk, but also at the interface e.g. between the oxide [6] and the silicon. Because only those centres which are in the SCR contribute to the bulk generation current, I_{BGC} depends on the voltage in the same way as the width of the SCR (eq. 2.24) :

$$I_{BGC} \propto \sqrt{V}. \tag{2.27}$$

It saturates when the applied voltage exceeds the depletion voltage.

The surface currents have many causes, which are not fully understood. In case of proper fabrication and handling the surface currents are negligible, but due to mechanical damage, humidity or other contamination of the diodes surface they can contribute significantly to the leakage current.

A characteristic of major concern is the so-called *breakdown* of a diode. If the reverse bias becomes greater than a certain voltage the current suddenly increases very rapidly. The common explanation for a breakdown is the avalanche process. In the electrical field, electrons and holes gain enough energy to generate further electron-hole pairs and thus an avalanche is triggered [6]. But the voltages usually

[5] $V_{bi} \approx 0.5$ V for SB-contacts [14] and about 0.7 V for ion-implanted diodes [15]. $(kT/q) = 25$ mV at room temperature.

[6] The manufacture of detectors and the function of the oxide are described in sec. 2.6.

applied to silicon detectors are too low for an avalanche breakdown. Only at the edges of the junction the electrical field can be high enough to cause a breakdown in this way. However, behaviour similar to a breakdown is often observed already at lower voltages. This might be due to voltage dependent surface effects or e.g. the SCR coming to close to the edge of the crystal. In any case the detector has to be operated above depletion voltage and below the breakdown voltage (see sec. 2.5).

If the diode is biased in forward direction a so-called *forward current* I_{for} flows. The forward current is irrelevant in terms of detector operation, but relevant with respect to some of the experimental techniques in use. Hence it is described in sec. 4.1.2.

2.2.3 Capacitance

For a diode a differential capacitance C is defined as

$$C = \frac{dQ}{dV}, \tag{2.28}$$

with dQ being the change of the space charge due to a change dV of the applied bias voltage [6]. The space charge Q of a SCR with a depth W is

$$Q = qN_{eff}AW, \tag{2.29}$$

with A being the area of the diode. Thus for a small change in dW one gets

$$dQ = qN_{eff}A\,dW. \tag{2.30}$$

The first-order derivative of V from eq. 2.24 gives

$$dW = \sqrt{\frac{\epsilon_S}{2qN_{eff}V}}\,dV. \tag{2.31}$$

Combined with eq. 2.30 the capacitance as function of the applied voltage V can be written as

$$C = \frac{dQ}{dV} = \frac{dQ}{dW}\frac{dW}{dV} = A\sqrt{\frac{\epsilon_S q N_{eff}}{2V}}. \tag{2.32}$$

Solving eq. 2.24 to

$$V = \frac{qN_{eff}}{2\epsilon_S}W^2 \tag{2.33}$$

and replacing V in eq. 2.32 with the right side one gets the capacitance as function of the depth W of the SCR

$$C = \epsilon_S\frac{A}{W}. \tag{2.34}$$

Of course the width of the SCR is limited by the thickness d of the detector and the equations eq. 2.30 to eq. 2.34 are valid only for $W < d$. If $W = d$ the detector is fully depleted and the corresponding voltage is called the voltage of full depletion V_{fd} (see eq. 2.25). The capacitance is then :

$$C = \epsilon_S\frac{A}{d}, \tag{2.35}$$

and will be fixed at this value also for voltages $V > V_{fd}$. [7] Because it depends only on the geometrical size of the diode it will be called hereafter *geometrical capacitance*.

2.3 Properties of Deep Energy Levels

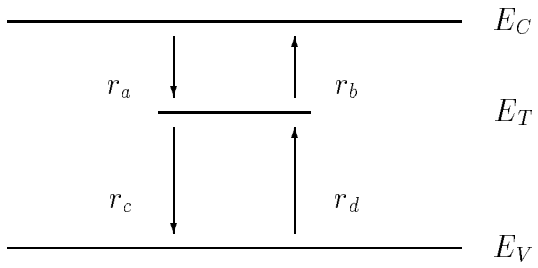

Figure 2.5: Emission and capture processes of an energy level E_T. Arrows present electron transitions.

The occupation of an energy level E_T [8] in the band gap of a semiconductor can be described as a statistical process [18]. Four competitive ways are possible to change the occupation (see fig. 2.5):

1. electron capture from the conduction band E_C : $r_a = c_n\, n\, p_T$, (2.36)
2. electron emission to the conduction band : $r_b = e_n\, n_T$, (2.37)
3. hole capture from the valence band E_V : (equivalent to electron emission to the valence band) $r_c = c_p\, p\, n_T$, (2.38)
4. hole emission to the valence band : (equivalent to electron capture from the valence band), $r_d = e_p\, p_T$. (2.39)

with

$r_{a,b,c,d}$	:	emission and capture rate respectively,
$c_{n,p}$	:	capture coefficients for electrons and holes,
$e_{n,p}$	:	emission probability for electrons and holes,
n, p	:	concentrations of free electrons and holes,
n_T	:	concentration of occupied levels,
p_T	:	concentration of non occupied levels,

and of course for the total trap concentration yields :

$$N_T = n_T + p_T. \tag{2.40}$$

[7] This simple picture holds only for detectors of simple geometry, e.g. great area A of electrodes in the same range as the area of the whole sample as realised for the PLUG-detector [16]. The capacitance of the samples used in this work often still decreases slightly if $V > V_{fd}$ due to lateral effects [17].

[8] As it is common practice in the following the differences $E_C - E_T$ and also $E_T - E_V$ are referred to as the activation energies of electrons, although indeed they are activation enthalpies.

The capture coefficients are product of the capture cross section $\sigma_{n,p}$ and the thermal velocity $v_{th,n,p}$ for electrons and holes respectively :

$$c_n = \sigma_n \, v_{th,n}, \; c_p = \sigma_p \, v_{th,p}. \tag{2.41}$$

The emission probabilities are given by :

$$e_n = \sigma_n \, v_{th,n} \, N_C \, \exp\left(\frac{-(E_C - E_T)}{k_B T}\right), \tag{2.42}$$

$$e_p = \sigma_p \, v_{th,p} \, N_V \, \exp\left(\frac{-(E_T - E_V)}{k_B T}\right), \tag{2.43}$$

where N_C and N_V are the state densities in the conduction band and valence band, respectively, and T is the temperature. Both the state density and the thermal velocity are also temperature dependent quantities. The thermal velocity is given by :

$$v_{th,n,p} = \sqrt{\frac{3k_B T}{m^*_{n,p}}}, \tag{2.44}$$

with $m^*_{n,p}$ being the effective mass of electrons and holes [9], respectively. The state densities are :

$$N_{C,V} = 2\left(\frac{2\pi m^*_{n,p} k_B T}{h^2}\right)^{3/2}. \tag{2.45}$$

The emission probabilities are often expressed in terms of the *intrinsic carrier concentration* n_i, which depends on the temperature as follows :

$$n_i = \sqrt{N_C N_V} \exp\left(-\frac{E_g}{2k_B T}\right). \tag{2.46}$$

Assuming $N_C \approx N_V$ eqs. 2.42 and 2.43 can be written as

$$e_n = \sigma_n \, v_{th,n} \, n_i \, \exp\left(\frac{E_T - E_i}{k_B T}\right), \tag{2.47}$$

$$e_p = \sigma_p \, v_{th,p} \, n_i \, \exp\left(\frac{E_i - E_T}{k_B T}\right), \tag{2.48}$$

with

$$E_i = \frac{E_C + E_V}{2} + \frac{k_B T}{2} ln\left(\frac{N_V}{N_C}\right). \tag{2.49}$$

While eqs. 2.42 and 2.43 determine the trap-level with respect to the valence band or the conduction band, eqs. 2.47 and 2.48 relate the trap level to the middle of energy gap.

Frequent use is made also of the inverse emission probability termed the emission time constant :

$$\tau_{n,p} = \frac{1}{e_{n,p}}. \tag{2.50}$$

[9] $m^*_n/m_0 = 1.08$, $m^*_p/m_0 = 0.558$

The change in concentration of occupied traps per time is the sum of the four competitive processes :

$$\frac{dn_T}{dt} = r_a - r_b - r_c + r_d. \tag{2.51}$$

For the SCR it is assumed that no free charge carriers exist ($n = p = 0$). Thus no capture will occur and eq. 2.51 is reduced to

$$\frac{dn_T}{dt} = -r_b + r_d. \tag{2.52}$$

Using eqs. 2.37, 2.39, 2.40 it follows

$$\frac{dn_T}{dt} = e_p N_T - (e_p + e_n) n_T. \tag{2.53}$$

Since it is $dn_T/dt = 0$ in steady-state the fraction of occupied traps f_T, i.e. the ratio n_T/N_T is then given by :

$$\frac{n_T}{N_T} = \frac{e_p}{e_p + e_n} = f_T. \tag{2.54}$$

Note that $f_T < 0.5$ if $e_n > e_p$ and vice versa $f_T > 0.5$ if $e_n < e_p$. In the following the emission probability will be called *emission rate* as it is common practice if deep level properties are discussed in terms of DLTS or TSC.

2.4 The Fermi - level

The *Fermi-level* E_F which is also called the electrochemical potential is defined by the following equation :

$$f(E) = \frac{1}{1 + exp(\frac{E - E_F}{k_B T})}. \tag{2.55}$$

$f(E)$ is the thermal equilibrium probability of occupancy for a state of energy E in a system of quantum states occupied by electrons (Fermi-Dirac-Statistic). E_F is determined by the condition that the number of occupied states for a given density of states distribution $g(E)$ must be equal to the number of electrons present :

$$n_o = \int_{-\infty}^{\infty} f(E) g(E) dE \tag{2.56}$$

In case of complete ionisation. i.e. $n \approx N_D$ or $p \approx N_V$ the Fermi-level can be described by eqs. 2.4 and 2.5.

However these equations hold only for the *electrically neutral bulk* (ENB) in thermal equilibrium. If an external voltage is applied to the junction, of course, this condition is not fulfilled and the Fermi-level does not describe the probability of occupancy. To describe the charge state of a trap with an energy level E_T in the SCR it is convenient to introduce a third energy E_1 associated with the properties of the level E_T by

$$E_1 = E_i + \frac{k_B T}{2q} ln \left(\frac{\sigma_p}{\sigma_n} \right), \tag{2.57}$$